processes

MDPI

Article

Energy, Exergy, and Economic Analysis of a New System for Simultaneous Power Production and Cooling Operating with an Ammonia–Water Mixture

Alejandro Pacheco-Reyes [1], José C. Jiménez-García [1], J. Alejandro Hernández-Magallanes [2], Raman Shankar [3] and Wilfrido Rivera [1,*]

[1] Instituto de Energías Renovables, Universidad Nacional Autónoma de México, Temixco 62580, Mexico
[2] Facultad de Ciencias Químicas, Universidad Autónoma de Nuevo León, San Nicolás de los Garza 66455, Mexico; jahem@ier.unam.mx
[3] Department of Aeronautical Engineering, MVJ College of Engineering, Channasandra, Bangalore 560067, India
* Correspondence: wrgf@ier.unam.mx; Tel.: +52-77-7362-0090 (ext. 29740)

Abstract: This paper presents the energy, exergy, and economic analysis of a new cogeneration cycle for the simultaneous production of power and cooling operating with an ammonia–water mixture. The proposed system consists of an absorption cooling system integrating a reheater, a separation tank, a compressor, a turbine, and an expansion valve. In addition, internal rectification is applied, improving the system's performance. Mass, energy, and exergy balances were applied to each system's component to evaluate its performance. Additionally, the costs of each component were determined based on economic equations, which take into account mass, heat flows, and temperature differences. A parametric analysis found that the system reached an energy utilization factor of 0.58 and an exergy efficiency of 0.26 using internal rectification at T_G = 120 °C, T_A = 30 °C, and T_E = 10 °C. The power produced by the turbine was 26.28 kW, and the cooling load was 366.8 kW. The output costs were estimated at 0.071 $/kW. The condenser was found to be the most expensive component of the system, contributing 28% of the total cost. On the other hand, it was observed that the generator was the component with the highest exergy destruction, with 38.16 kW.

Keywords: absorption cooling system; cogeneration; power and cooling; Goswami cycle

Citation: Pacheco-Reyes, A.; Jiménez-García, J.C.; Hernández-Magallanes, J.A.; Shankar, R.; Rivera, W. Energy, Exergy, and Economic Analysis of a New System for Simultaneous Power Production and Cooling Operating with an Ammonia–Water Mixture. *Processes* **2024**, *12*, 1288. https://doi.org/10.3390/pr12071288

Academic Editors: Mateo Bašić and Dejan Jokić

Received: 28 May 2024
Revised: 15 June 2024
Accepted: 19 June 2024
Published: 21 June 2024

1. Introduction

Currently, world society is experiencing great difficulties, such as water scarcity, the inability to supply 100% of energy demand, and high rates of environmental pollution, among others. On the other hand, according to the United Nations, the world population increased from 2.6 billion in 1950 to 8 billion in mid-November 2022. It is estimated that by 2050, the world population will be 9.7 billion [1]. These are quite alarming figures since the problems mentioned above will increase considerably as the world population increases. Environmental pollution from using fossil fuels for power generation is an urgent issue that must be addressed immediately. Renewable energy sources, energy efficiency studies, and developing and improving energy conversion systems are viable alternatives to combat these problems. According to the International Energy Agency (IEA) [2], energy production increased by 2% between 2018 and 2019, with the largest increases recorded for coal and natural gas use. Renewable sources also were on the rise, as solar energy increased by 14%, wind energy by 12%, and hydroelectricity remained stagnant at 15 EJ. Despite these gains, fossil fuels still accounted for 81% of energy production, with oil contributing the most with 190 EJ. A significant portion of this energy is used to meet the demand for refrigeration, which is essential in various sectors, from transportation to medicine. According to the United Nations Environment Program [3], the energy demand for building cooling tripled from 1990 to 2016, increasing from 600 TWh to 2000 TWh. It was observed that from 50%

to 80% of the energy in buildings is used for air conditioning. Currently, 17% of the total energy produced is consumed by refrigeration equipment. In 2018, refrigeration systems were estimated to consume 3900 TWh/year of electricity worldwide.

Concerning energy systems, in the last decades, several investigations have been addressed to develop more efficient energy conversion systems, aiming to reduce their impact on the environment. In this regard, polygeneration systems have gained the scientific community's attention due to their high versatility and the possibility to simultaneously produce several useful effects, mainly power, cooling, and heating. Moreover, the integration of renewable energies or industrial waste heat with polygeneration has resulted not only in economically feasible systems but also in lower environmental impacts.

1.1. Analyses Based on the Goswami Cycle

As for power and cooling production, the first reference cycle is the one proposed by Goswami [4]. This system is based on the operating principle of a Rankine cycle and an absorption refrigeration cycle. This cycle was proposed to use an ammonia–water mixture in the absorption components and ammonia vapor in the turbine. Following the configuration proposed by Goswami, a system producing 2 MW of power could supply up to 50 tons of cooling. The cycle's first-law efficiency using a heat source near 193 °C was approximated to 32%.

The Goswami cycle deals with the production of different energy outputs (power and cooling); on this subject, Vijayaraghavan and Goswami [5] and Sadrameli and Goswami [6] developed a thermodynamic analysis to obtain the appropriate equations to objectively evaluate polygeneration systems using basic concepts of thermodynamics applied to some specific cases. Such methodology was adopted by Hasan et al. [7] to analyze the Goswami cycle from the perspective of the first and second laws of thermodynamics, finding efficiencies of 16.9% and 65.4%, respectively, while a power production and a cooling load of 47.2 kJ/kg_{sol} and 3.5 kJ/kg_{sol}, respectively, was achieved. They also determined that the absorber was the component with the highest irreversibilities, contributing 44% of the total. Although the Goswami cycle is designed to produce both power and cooling, its configuration benefits the power over the cooling production. To increase the cooling production compared to the Goswami cycle, Rivera et al. [8] proposed two configurations to boost the cooling load over the power production. The first configuration presented a split flow at the rectifier outlet, while the second cycle had a direct flow bleed from the turbine. Both models had higher cooling loads and energy utilization factors (EUFs) than the Goswami cycle, but the cycle with the turbine bleed presented the best performance. This cycle decreases the turbine power by 23% but increases the cooling production by almost six times compared to the Goswami cycle.

An extensive thermodynamic analysis of the Goswami cycle driven at temperatures between 100 and 350 °C was performed by Demirkaya et al. [9]. The study included the assessment of several operation and configuration parameters on the cycle performance, finding that efficiencies between 25 and 31% and 60 and 80% for the first and second perspectives, respectively, could be achieved by the cycle. This study considered an ammonia–water working fluid, like many others in the literature. On the contrary, Vijayaraghavan and Goswami [10] analyzed several mixtures based on organic fluids as the working fluid in a Goswami cycle. The analysis included ammonia, methane, propane, n-decane, isobutane, and n-dodecane. Among the characteristics analyzed for the working fluids are corrosivity, toxicity, flammability, and stability. The performance achieved with the organic fluids was found to be poorer than that with the ammonia–water mixture in terms of efficiencies and cooling temperatures.

1.2. Analyses Based on the Kalina Cycle

In addition to the Goswami cycle, the Kalina cycle is another well-known reference for power cycles driven by heat sources at temperatures lower than those required by the steam Rankine cycle. The original Kalina cycle has been modified through the years

to enable the production of additional energy effects, such as cooling. A configuration for power and cooling involving a Kalina cycle usually integrates an absorption cooling cycle. In this regard, Wang et al. [11] proposed a configuration of such a system to produce power up to 35.8 kW and cooling up to 75.1 kW. This system operated with an ammonia–water mixture and a heat source at 200 °C and obtained energy and exergy efficiencies of 13.72% and 5.40%, respectively. Notably, this cycle's cooling/power rate is much more significant than that in the Goswami cycle. Another configuration of Kalina/absorption cycles was analyzed by Cao et al. [12], who developed an analysis of a system composed of a Kalina cycle and an absorption refrigeration cycle. The analysis showed that 89.5 kW of power and an exergy efficiency of 25.7% could be produced at 129.6 °C and 80% of solution concentration.

A couple of configurations of a Kalina/absorption cycle were proposed by Feng et al. [13]. Such configurations were named the double-pressure series cycle (DSC) and the double-pressure parallel cycle (DPC). Comparing both models under similar conditions, the DPC cycle had energy and exergy efficiencies of 30.1% and 23.8%, respectively. In comparison, the DSC cycle reached energy and exergy efficiencies of 34.44% and 24.63%, respectively. For both models, increasing the source temperature and the solution concentration in the NH_3-H_2O mixture benefited the system performance.

Instead of an absorption system, Seckin [14] integrated an ejector system into the Kalina cycle for cooling purposes. An ammonia–water mixture was used as the working fluid while R134a, R152a, and R290 were tested on the ejector system. The study determined that the highest thermal efficiency and cooling loads were obtained using R290, while the highest exergy efficiency was obtained using R134a.

The integration of a Kalina cycle, an absorption system, and an electrolyzer for the production of power, cooling, and hydrogen was proposed by Azariyan et al. [15]. The thermodynamic analysis considered that this polygeneration cycle was driven by geothermal energy, finding that at 400 °C, the system could produce 1272 kg/h of hydrogen, 80.11 kW of power, and 258.6 kW of cooling, with energy and exergy efficiencies of 22.2% and 21.3%, respectively.

Due to the complexity inherent to such systems, the vast majority of polygeneration studies in the literature rely on theoretical analyses. Among the few experimental studies, Kumar et al. [16] investigated the combination of an absorption system and a Kalina cycle using low-grade energy. The analysis was carried out using energy and exergy approaches, finding that at a generation temperature of 133 °C, the first and second laws' efficiencies were 13% and 48%, respectively, while the power and cooling load were 2.2 kW and 15.26 kW, respectively. The modeled system can adjust the power or cooling load as required.

1.3. Alternative Cycles

The proposals for new polygeneration cycles should be addressed through a systematic design method. In the case of power and cooling cycles, Zhang and Lior [17] proposed a methodology for the thermal design of such systems using binary working fluids, such as the NH_3-H_2O mixture. Moreover, following that methodology, a series of power/cooling models with different arrangements was developed. The thermal efficiency for the base case studied was nearly 28%, while the exergy efficiency varied between 55 and 60%. That system achieved a cooling load of 191.66 kW and 783.75 kW of power with a heat source at 450 °C.

Some alternative cycles for simultaneous power and cooling production have also been proposed in the literature. Suleman et al. [18] developed a system integrating two organic Rankine cycles, an absorption chiller, and a drying system. Such a system is based on solar and geothermal energy and can be useful for power, cooling, and drying. The energy and exergy efficiencies of the integrated system were 54.7% and 76.4%, respectively. Rather, Ayou et al. [19] analyzed the effect of adding a mechanical and a thermal compressor to a simultaneous power and cooling cycle. It was found that this configuration contributed to

reducing the energy supplied to the generator. The system produced 9.4 kW of power and a cooling load of 64.1 kW at −12 °C. The energy and exergy efficiencies were reported as 12.2% and 60.7%, respectively. The second-law analysis showed that the absorber and the heat exchanger had the highest irreversibilities, contributing 28% and 30.9%, respectively, to the total irreversibility.

The working fluid utilized in an energy system has a significant impact on the system's performance. Research on the assessment of several working fluids for an alternative system to produce power, cooling, hydrogen, and fresh water was carried out by Cao et al. [20]. This system included a flash-binary geothermal plant and an organic flashing cycle for power and cooling. The working fluids analyzed were R123, R600, R1234yf, and R1234ze(e). It was found that the maximum cooling load was obtained with the fluids R123 and R1234ze(e), while the maximum power generation and exergy efficiency were obtained with R600 and R1234yf.

Diverse strategies for enhancing the performance of polygeneration systems have been reported in the literature; among them, Shankar and Rivera [21] integrated a dual and a triple cogeneration cycle using an ammonia–water mixture for power/cooling production. In addition to conventional components, the proposed system had an expansion valve and a separator tank to produce more working fluid, which was introduced to a second turbine to increase power production. The work obtained from both turbines was 67.25 kW, while the cooling load and energy utilization factor were 75.12 kW and 0.33, respectively.

An alternative strategy proposed by Parikhani et al. [22] aimed to take advantage of the solution leaving the generator in an absorption-power cycle to produce additional ammonia vapor available for cooling production. The power produced was 161.2 kW, and the cooling load was 221.4 kW. The thermal and exergy efficiencies were 16.4% and 28.95%, respectively. Following such a strategy, Shankar and Rivera [23] passed this solution through an expansion valve and later through a separator to obtain an extra amount of refrigerant. This ammonia vapor at intermediate pressure was expanded by a low-pressure turbine, producing an extra amount of power. The energy and exergy efficiencies were 47% and 43.87%, respectively. The total power produced was 20.28 kW, while the cooling load was 354.21 kW.

1.4. Economic Analyses

Besides the technical performance, an additional approach to take into consideration while assessing new polygeneration cycles is the economic perspective. Several studies on economic analyses of polygeneration systems have been reported, including different methods and parameters to consider. In this regard, Dahad et al. [24] evaluated a power and cooling system with a power capacity near 158.3 kW and a cooling load of approximately 1084 kW. Notably, the proposed system was more suitable for power than cooling. The system had a first-law efficiency of 41.3% and an exergy efficiency of 27.4%. The cost for cooling was 48.5 $/GJ, while for power production it was 97.16 $/GJ. An exergy analysis showed that the absorber had the highest exergy destruction, contributing 93.4 kW. On the other hand, Kordlar and Mahmoud [25] carried out the economic assessment of a system driven by geothermal energy composed of an organic Rankine cycle and an absorption cooling system. Three optimization cases were analyzed, considering (i) the maximum energy efficiency, (ii) the maximum exergy efficiency, and (iii) the lowest cost. It was found that, when optimizing the cost, the unit cost for total products was 20.4% and 24.3% lower than the unit cost for the total products when optimizing energy and exergy efficiencies, respectively. On the other hand, the analysis of a system based on a Kalina cycle and an ejector refrigeration cycle for power and cooling was carried out by Ghaebi et al. [26], who found that when optimizing the energy efficiency (20.4%), the system achieved an exergy efficiency of 16.69% and a product cost of 2466.3 $/MWh. Ghaebi et al. [27] also investigated a trigeneration system for power, cooling, and heating production. The proposed system is based on the absorption refrigeration cycle and utilizes a geothermal heat source and liquefied natural gas for energy recovery. The system evaluation was based on the power,

cooling, and heating outputs, as well as on first- and second-law efficiencies and the sum unit cost of the products (SUCP), which were equivalent to 405.1 kW, 1109 kW, 35.3 kW, 85.92%, 18.52%, and 68.76 $/GJ, respectively.

To enhance the efficiency of the power/cooling cycles, Wang et al. [28] proposed a theoretical system based on the absorption power cycle and a booster-assisted ejector refrigeration system to be driven by low-grade heat sources. The analysis included the energy, exergy, and exergoeconomic approaches, finding that the booster compressor in the ejector system improved the energy efficiency regarding traditional absorption power cycles. The system reached energy and exergy efficiencies of 21.7% and 52.2%, respectively, while the sum unit cost of the products was 93.52 $/GJ. Similarly, Abam et al. [29] analyzed a modified Kalina cycle for power and cooling. The theoretical system's cooling load and power reached 1077 kW and 291 kW, respectively, while the energy and exergy efficiencies were 16.97% and 8.15%. The economic analysis showed that the unit cost of energy at five years was 0.0134 $/kWh.

As can be seen from the bibliographic review, although some systems have been proposed for the simultaneous production of power and cooling, none of them considered integrating a separation tank and a compressor to produce more ammonia refrigerant to enhance the system's performance. Therefore, this study proposes a novel thermodynamic cycle designed for simultaneous power and cooling generation employing an ammonia–water mixture as the working fluid, whose novelty is the incorporation of an expansion valve, a separator, and a compressor to enhance the refrigerant mass flow rate, taking advantage of the ammonia remaining in the solution after the desorption process; such a stream undergoes a throttling and separation process to generate an additional quantity of vapor with a high concentration of ammonia [8,22,23]. The produced vapor is subsequently compressed until reaching the highest pressure in the system. By increasing the mass flow rate in both the turbine and the evaporator, benefits will accrue in power generation and cooling effects. The proposed system is comprehensively analyzed from the energy, exergy, and economic perspectives. Furthermore, the performance of this system is compared with similar studies previously reported in the literature.

2. System Description

2.1. Goswami Cycle

Goswami proposed a cycle to produce power and cooling simultaneously. The cycle can be considered a combination of a Rankine cycle and an absorption cooling cycle, as can be seen in Figure 1. An ammonia–water solution in the liquid phase leaving the absorber (1) is pumped (2) to the generator, (3) passing first through the economizer. Heat is supplied to this component to evaporate part of the solution with high ammonia concentration (7), which then passes to the rectifier, where it is rectified, leaving the component as almost pure ammonia (9). Then, the ammonia vapor is reheated in the reheater, increasing its temperature before entering the turbine (10). In the turbine, the ammonia expansion produces an amount of power, reducing its pressure and temperature before entering the cooler (11). In this component, the cooling effect is produced, and the ammonia in the vapor phase leaving this component (12) is absorbed by the solution coming from the generator at low ammonia concentration (4), preheating first in the economizer the solution with intermediate ammonia solution concentration. The solution at a lower temperature, on leaving the economizer (5), passes through a valve that reduces its pressure before entering the absorber. In this component, ammonia vapor absorption takes place, producing the solution with an intermediate solution concentration and starting the cycle again.

One of the first modifications of the Goswami cycle was internal rectification [30]. Figure 1b shows the Goswami cycle but with internal rectification. This consists of the rectification process using one of the internal currents of the cycle, specifically the one leaving the pump. The mass flow rate at the pump outlet is divided; a fraction enters the economizer, and the remaining fraction passes through the rectifier. The fraction entering the rectifier increases its temperature due to the heat transfer from the vapor entering the

rectifier, while the fraction going to the economizer also increases its temperature by the heat transfer from the hot solution coming from the generator. The internal rectification benefits the system since the heat delivered from the rectification process is used to preheat the solution entering the generator, thus decreasing the heat supplied to this component and increasing the system's efficiency.

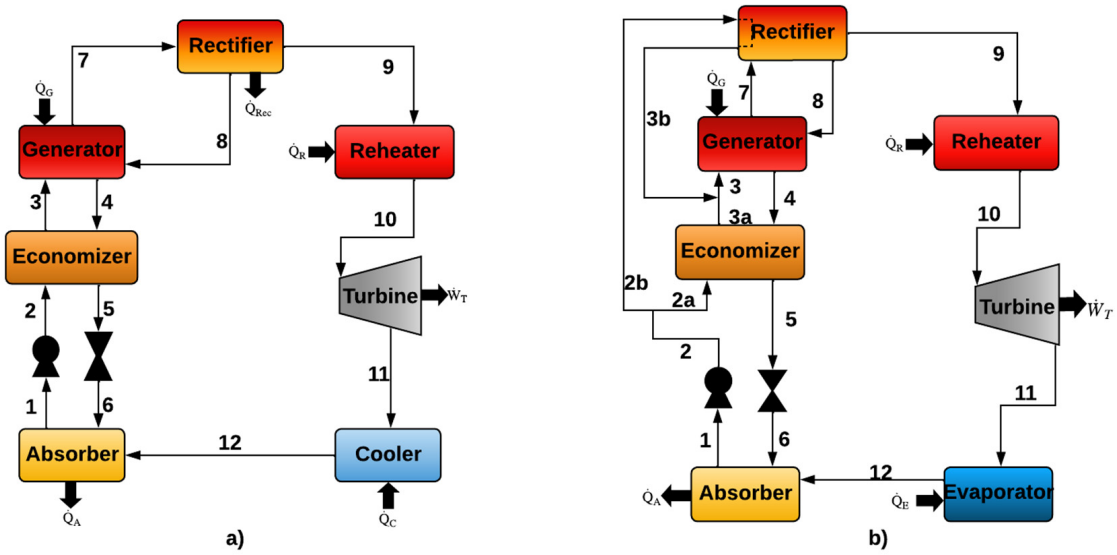

Figure 1. Goswami cycle, (**a**) without internal rectification, and (**b**) with internal rectification.

2.2. Proposed System

Figure 2a shows a schematic diagram of the proposed cogeneration cycle for power and cooling (CCPC). An ammonia–water solution leaving the absorber (1) is pumped to the economizer (2), where it is preheated before entering the generator (3). In the generator, a quantity of heat ($\dot{Q}_G$) is supplied to produce vapor with a high ammonia concentration and a liquid solution with a low ammonia concentration. This liquid solution leaves the generator (4) and passes through a valve (5), reducing its pressure and producing a flashing effect. In the separation tank, an extra amount of vapor with a high ammonia concentration and saturated liquid at the lowest ammonia concentration are produced. The solution leaving the separation tank (6) passes through the economizer (7), preheating the solution to the generator. Then, the solution reduces its pressure before entering the absorber (8). On the other hand, the saturated vapor leaving the separator (9) is compressed, increasing its pressure and temperature (10). At these conditions, the vapor mixes with the ammonia vapor produced in the generator (11) before entering the rectifier (12). In this component, heat ($\dot{Q}_R$) is removed to condense the water contained in the vapor, which returns to the generator (13). The ammonia vapor—almost pure—leaving the rectifier (14) is reheated in the reheater utilizing an amount of heat ($\dot{Q}_R$), increasing its temperature before entering the turbine (15). In the turbine, an amount of power ($\dot{W}_T$) is produced by the working fluid expansion. The working fluid leaving the turbine at a lower pressure and temperature (16) passes to the condenser, where it is condensed, delivering an amount of heat ($\dot{Q}_C$). The liquid ammonia leaving the condenser at saturated conditions (17) is precooled in the precooler (18). Then, the ammonia is expanded in the expansion valve, reducing its pressure and temperature before entering the evaporator (19). In the evaporator, the working fluid produces a cooling effect by removing an amount of heat ($\dot{Q}_E$). The ammonia leaving the evaporator (20) as a saturated vapor is used to precool the stream going to the evaporator. Then, the ammonia goes to the absorber (21), where it is absorbed by the solution from the separation tank, starting the cycle again. Figure 2b shows the proposed cycle but with internal rectification in a similar way to the Goswami cycle.

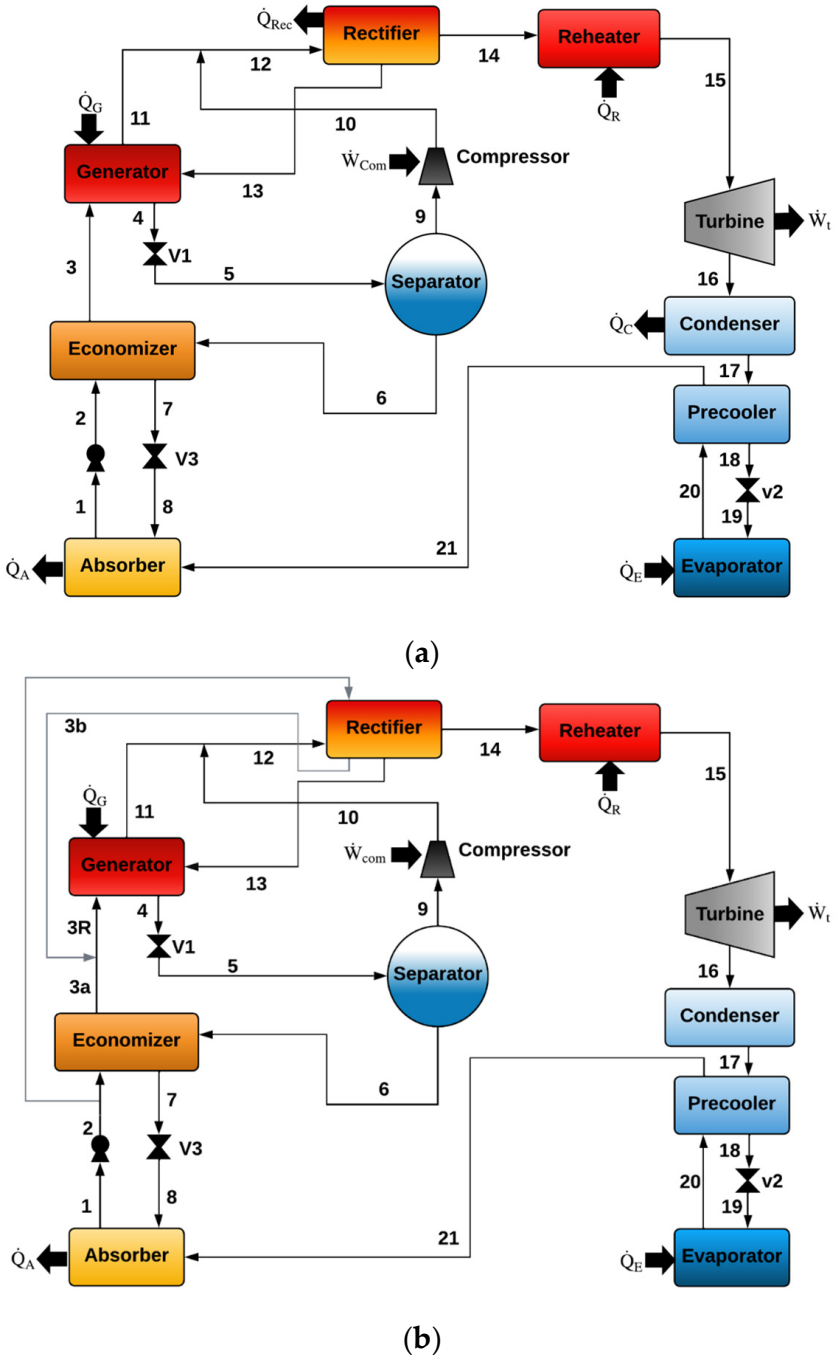

Figure 2. Schematic diagram of the proposed CCPC without (**a**) and with (**b**) internal rectification.

Comparing the Goswami cycle with the proposed system, and from Figures 1 and 2, it can be observed that a separator, a compressor, a condenser, and an evaporator were added to the proposed system, and the cooler was replaced with a precooler. The separator and the compressor have the purpose of increasing the ammonia refrigerant produced by taking advantage of the relatively high ammonia concentration leaving the generator; the condenser and evaporator have the purpose of increasing the amount of cooling produced by the system by using the latent heat of evaporation of the refrigerant in the evaporator.

In both cycles, with and without internal rectification, heat is supplied to the systems in the generator and in the reheater. Because these cycles operate at relatively low temperatures, the heat supplied to the system could be from renewable energies, such as solar or geothermal, and also from industrial waste heat.

3. Mathematical Model

Mass, energy, and exergy balances were realized to determine the thermodynamic states for each component. With the thermodynamic properties at the input and output of each component, the energy utilization factor (EUF) was determined. The EUF is a parameter analogous to the first-law efficiency since it indicates the amount of useful energy produced and the total energy supplied to the system. However, this parameter does not consider whether the useful energy is heat or power. An alternative performance parameter to avoid adding different kinds of energy outputs is the exergy efficiency (η_{Ex}), defined as the useful exergy obtained from the system divided by the total exergy supplied to the system [8]. Table 1 shows the balance equations for each system's component.

Table 1. Mass, energy, and exergy balances for each system's component.

Mathematical Model	
Generator $\dot{m}_3 + \dot{m}_{13} = \dot{m}_4 + \dot{m}_{11}$ $\dot{m}_3 X_3 + \dot{m}_{13} X_{13} = \dot{m}_4 X_4 + \dot{m}_{11} X_{11}$ $\dot{m}_3 h_3 + \dot{m}_{13} h_{13} + \dot{Q}_G = \dot{m}_4 h_4 + \dot{m}_{11} h_{11}$ $Ex_{dG} = \dot{Q}_G\left(1 - \frac{T_0}{T_G}\right) + \dot{m}_3(h_3 - T_0 s_3) + \dot{m}_{13}(h_{13} - T_0 s_{13}) -$ $\dot{m}_4(h_4 - T_0 s_4) - \dot{m}_{11}(h_{11} - T_0 s_{11})$	Reheater $\dot{m}_{14} h_{14} + \dot{Q}_R = \dot{m}_{15} h_{15}$ $Ex_{dR} = \dot{Q}_R\left(1 - \frac{T_0}{T_R}\right) + \dot{m}_{14}[(h_{14} - h_{15}) - T_0(s_{14} - s_{15})]$
Economizer $\dot{m}_2 h_2 + \dot{m}_6 h_6 = \dot{m}_3 h_3 + \dot{m}_7 h_7$ $Ex_{dec} = \dot{m}_2[(h_2 - h_3) - T_0(s_2 - s_3)] + \dot{m}_6[(h_6 - h_7) - T_0(s_6 - s_7)]$	Turbine $\dot{W}_t = \eta_t(\dot{m}_{15} h_{15} - \dot{m}_{16} h_{16})$ $Ex_{dt} = \dot{m}_{14}[(h_{15} - h_{16}) - T_0(s_{15} - s_{16})] - \dot{W}_t$
Absorber $\dot{m}_{21} + \dot{m}_8 = \dot{m}_1$ $\dot{m}_{21} X_{21} + \dot{m}_8 X_8 = \dot{m}_1 X_1$ $\dot{m}_{21} h_{21} + \dot{m}_8 h_8 = \dot{m}_1 h_1 + \dot{Q}_A$ $Ex_{dA} = \dot{m}_{21}(h_{21} - T_0 s_{21}) + \dot{m}_8(h_8 - T_0 s_8) - \dot{m}_1(h_1 - T_0 s_1) -$ $\dot{Q}_A\left(1 - \frac{T_0}{T_A}\right)$	Condenser $\dot{m}_{16} h_{16} = \dot{m}_{17} h_{17} + \dot{Q}_c$ $Ex_{dc} = \dot{m}_{16}[(h_{16} - h_{17}) - T_0(s_{16} - s_{17})] - \dot{Q}_c\left(1 - \frac{T_0}{T_c}\right)$
Pump $\dot{W}_P = \dot{m}_1(h_2 - h_1)/\eta_P$ $Ex_{dp} = \dot{W}_p + \dot{m}_1[(h_1 - h_2) - T_0(s_1 - s_2)]$	Precooler $\dot{m}_{17} h_{17} + \dot{m}_{20} h_{20} = \dot{m}_{18} h_{18} + \dot{m}_{21} h_{21}$ $Ex_{dPr} = \dot{m}_{17}[(h_{17} - h_{18}) - T_0(s_{17} - s_{18})] + \dot{m}_{20}[(h_{20} - h_{21}) - T_0(s_{20} - s_{21})]$
Separator $\dot{m}_5 = \dot{m}_9 + \dot{m}_6$ $\dot{m}_5 X_5 = \dot{m}_9 X_9 + \dot{m}_6 X_6$ $Ex_{dS} = \dot{m}_5(h_5 - T_0 s_5) - \dot{m}_9(h_9 - T_0 s_9) - \dot{m}_6(h_6 - T_0 s_6)$	Evaporator $\dot{m}_{19} h_{19} + \dot{Q}_E = \dot{m}_{20} h_{20}$ $Ex_{dE} = \dot{Q}_E\left(1 - \frac{T_E}{T_0}\right) + \dot{m}_{19}[(h_{19} - h_{20}) - T_0(s_{19} - s_{20})]$
Compressor $\dot{W}_{com} = \dot{m}_9(h_{10} - h_9)/\eta_{com}$ $Ex_{com} = \dot{W}_{com} + \dot{m}_9[(h_9 - h_{10}) - T_0(s_9 - s_{10})]$	Energy Utilization Factor $EUF = \frac{\left(\dot{W}_T + \dot{Q}_E\right)}{\left(\dot{W}_B + \dot{W}_c + \dot{Q}_G + \dot{Q}_R\right)}$
Valves $\dot{m}_{in} h_{in} = \dot{m}_{out} h_{out}$ $Ex_{dv} = \dot{m}_{in}[(h_{in} - h_{out}) - T_0(s_{in} - s_{out})]$	Exergy efficiency $\eta_{Ex} = \frac{\dot{W}_T + \left(\frac{T_O - T_E}{T_E}\right)\dot{Q}_E}{\dot{Q}_G\left(1 - \frac{T_O}{T_G}\right) + \dot{Q}_R\left(1 - \frac{T_O}{T_R}\right) + \dot{W}_B + \dot{W}_C}$
Rectifier $\dot{m}_{12} = \dot{m}_{14} + \dot{m}_{13}$ $\dot{m}_{12} h_{12} = \dot{m}_{14} h_{14} + \dot{m}_{13} h_{13} + \dot{Q}_{Rec}$ $Ex_{dRec} = \dot{m}_{12}(h_{12} - T_0 s_{12}) - \dot{m}_{14}(h_{14} - T_0 s_{14}) -$ $\dot{m}_{13}(h_{13} - T_0 s_{13}) - \dot{Q}_R\left(1 - \frac{T_0}{T_{Rec}}\right)$	

To evaluate the proposed system, a computational model was developed using the EES (Engineering Equation Solver V10.836-3D) software. This software has been chosen because it has the validated subroutines of the working mixture with which the CCPC operates.

3.1. Assumptions

The typical considerations used in the literature [21,23,25] for analyzing this type of system were adopted to develop the mathematical model. These considerations are the following:

- The system operates in steady-state conditions.
- There are no temperature or pressure losses in the component connections.
- The processes in the valves are considered isenthalpic.
- The working fluid in states 1, 4, 6, 13, and 17 is saturated liquid.
- The working fluid in states 9, 11, and 14 is considered saturated vapor.
- The temperature and pressure of the dead state are 25 °C and 101.325 kPa.

3.2. Input Data

For the system evaluation, different operating conditions were analyzed by varying parameters such as generation, absorption, condensation, evaporation, and reheating (ΔR) temperatures. Table 2 shows the ranges of the variables analyzed in the modeling and some other parameters of interest.

Table 2. Operating range of the analyzed variables.

Variable	Operation Range	Increment
T_E (°C)	0–16	2
$T_A = T_C$ (°C)	20–40	2.5
T_G (°C)	100–140	5
ΔR (°C)	0–50	10
P_G/P_S (-)	1–10	1
X_A (-)	0.44–0.60	0.02
ε_{Ec} (-)	0.90	-
ε_{Pr} (-)	0.90	-
η_T (-)	0.90	-
η_P (-)	0.90	-
η_{Com} (-)	0.90	-
$\dot{m}_1$ (kg/s)	1	-

3.3. Flowchart Diagram of the Mathematical Model

To solve the computational model, the variables to be analyzed are introduced to the model together with the considered assumptions. With this information, the model can determine the remaining properties for each state. Determining each thermodynamic state requires three parameters: either thermodynamic properties or fluid conditions. Figure 3 shows the flowchart of the mathematical model developed. It starts with the input data and ends with calculating the heat loads, powers, and efficiency parameters, such as the EUF, η_{Ex}, and I.

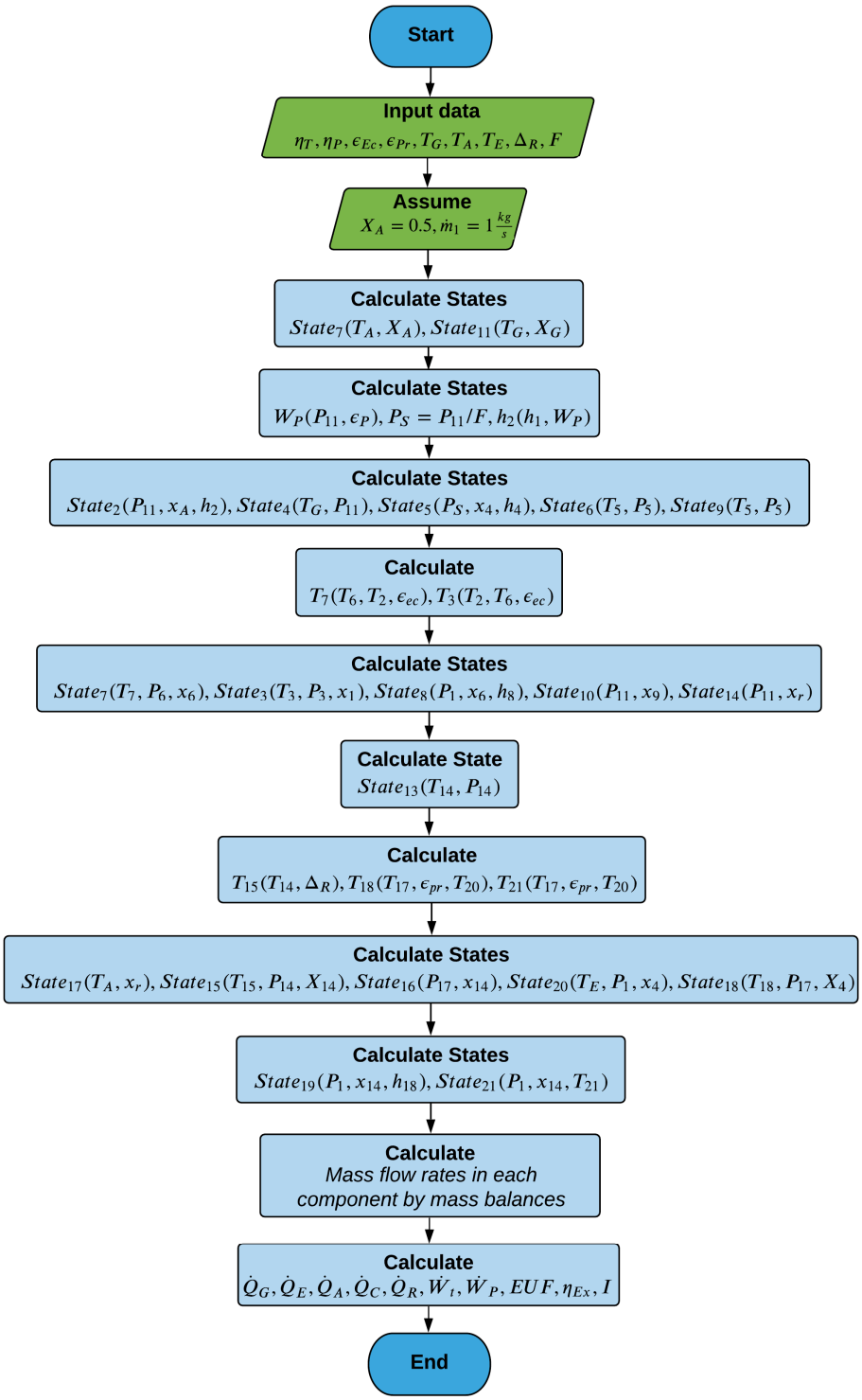

Figure 3. CCPC solution flowchart.

4. Economic Study

Equations (1)–(11) determine the cost for each component. These equations have previously been used for similar systems, such as power generation, cooling systems, and plants operating with the Kalina cycle [23,29,31]. However, the system components' costs have changed since the equations were proposed due to economic inflation. Therefore, the Chemical Engineering Plant Cost Index (*CEPCI*) is used to update the costs for a more accurate economic study [32].

Generator cost [23,29]:

$$Z_G = 309.14\left[\frac{\dot{Q}_G}{0.2\Delta T_G}\right]^{0.85} \quad (1)$$

Reheater cost [23]:

$$Z_R = 16000\left[\frac{A_R}{100}\right]^{0.60} \quad (2)$$

Turbine cost [23,24,26,29,31]:

$$Z_T = 4405\left[\dot{W}_T\right]^{0.70} \quad (3)$$

Condenser cost [23,29]:

$$Z_C = 516.62\left[\frac{\dot{Q}_C}{0.15\Delta T_C}\right] \quad (4)$$

Precooler cost [23]:

$$Z_{Pr} = 309.14\left[\frac{\dot{Q}_{Pr}}{0.2\Delta T_{Pr}}\right]^{0.85} \quad (5)$$

Evaporator cost [23,29]:

$$Z_E = 309.14\left[\frac{\dot{Q}_E}{0.2\Delta T_E}\right]^{0.85} \quad (6)$$

Absorber cost [23]:

$$Z_A = 516.62\left[\frac{\dot{Q}_A}{0.15\Delta T_A}\right] \quad (7)$$

Pump cost [23,29,31]:

$$Z_P = 1120\left[\dot{W}_P\right]^{0.80} \quad (8)$$

Economizer cost [23]:

$$Z_{Ec} = 12500\left[\frac{A_{Ec}}{100}\right]^{0.60} \quad (9)$$

Valve cost [26]:

$$Z_V = 114.5\left[\dot{m}_v\right] \quad (10)$$

Compressor cost [27]

$$Z_{Com} = 9624.2\left[\dot{W}_{Com}\right]^{0.46} \quad (11)$$

The component's area is determined by Equation (12):

$$\dot{Q}_i = U_i A_i \Delta TML \quad (12)$$

where ΔTML is the logarithm medium temperature, and it can be calculated by Equation (13):

$$\Delta TML = \frac{\Delta T_1 - \Delta T_2}{\ln(\Delta T_1/\Delta T_2)} \quad (13)$$

By knowing the cost of each component, the total investment cost of the system can be determined by Equation (14) since it is the sum of the cost of all the components.

$$Z_{Total} = \sum Z_{Components} \quad (14)$$

The *CEPCI* was used in Equation (15), and the costs were updated until 2019.

$$Z_{2019} = Z_{Total} \times \frac{CEPCI_{2019}}{CEPCI_{2000}} \quad (15)$$

where Z_{Total} is the cost of the system, $CEPCI_{2000}$ = 394.1, and $CEPCI_{2019}$ = 652.9.

Another important aspect to consider in the economic analysis is the degradation of the components, which affects the system's performance. The following equation was used to determine the turbine degradation, which gave a value of 1.69% in plant lifetime, which was included in the analysis [33]. Because the cycle is a closed system and the heat exchangers were considered made of stainless steel, no corrosion and fouling effects were considered. Therefore, the system degradation was considered negligible in the heat exchangers.

$$HPST\ degradation = \left(\frac{\eta_{HPST,is(MTP)} - \eta_{HPST,is(AP)}}{\eta_{HPST,is(MTP)}} \right) \times 100 \quad (16)$$

where:

$$\eta_{HPST,is} = \left(\frac{h_{15} - h_{16,ac}}{h_{15} - h_{16,is}} \right) \times 100 \quad (17)$$

To carry out a more detailed economic analysis, the operating time of the system must be known, which is considered to be 10 h per day with a plant lifetime of 25 years. The interest rate was considered to be 7.2% [34].

The capital recovery factor (*CRF*) can be determined by Equation (18) by knowing the parameters mentioned above.

$$CRF = \frac{i(1+i)^n}{(1+i)^n - 1} \quad (18)$$

The sinking fund factor (*SFF*) can be estimated as follows:

$$SFF = \frac{i}{(1+i)^n - 1} \quad (19)$$

The annual capital cost can be calculated once the two previous parameters have been determined.

$$ACC = Z_{2019} \times CRF \quad (20)$$

The salvage value (*SV*) can be calculated as follows:

$$SV = 0.20 \times Z_{2019} \quad (21)$$

Meanwhile, the annual salvage value (*ASV*) can be estimated using Equation (22).

$$ASV = SV \times (SFF) \quad (22)$$

The maintenance cost (*CM*) per annum is considered 10% of the annual capital cost.

$$CM = ACC \times 0.1 \quad (23)$$

Therefore, the annual total cost (*ATC*) is the sum of the annual capital cost plus the maintenance cost per annum minus the annual salvage value, expressed by the following equation:

$$ATC = ACC + MC - ASV \quad (24)$$

Considering the annual equivalent of electrical energy, the cooling power must be transferred in terms of electrical energy to determine the cost of the cogeneration products.

For this reason, a *COP* of 2.5 is considered [23], with which the following equation gives the cogeneration cost of the products:

$$CCCP = \frac{ATC}{W_{Ta} + Q_{Ee}} \tag{25}$$

5. Results

5.1. Analysis of the CCPC as a Function of the Generation Temperature

Figure 4 shows the ammonia vapor mass flow rates produced in the generator, separator, and the flow entering the turbine.

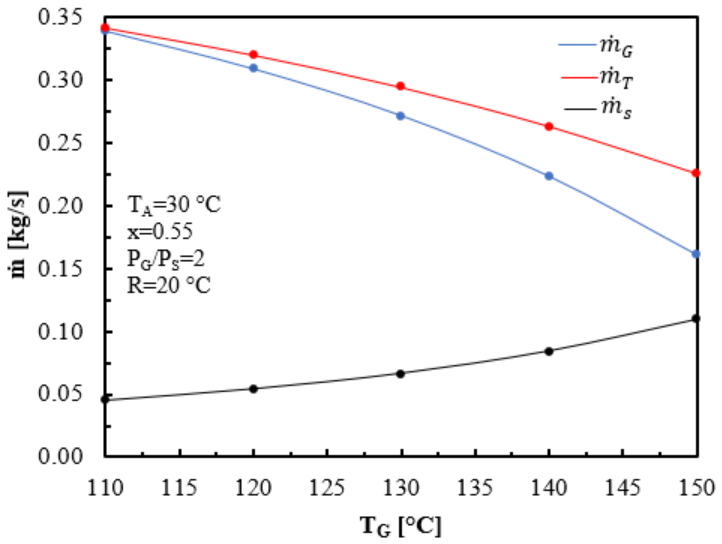

Figure 4. Generator mass flows as a function of the generator temperature.

For the CCPC, the increase in the generation temperature limits the refrigerant desorption in the generator due to heat losses to the environment. On the other hand, when the production of the ammonia vapor in the generator decreases, the mixture concentration does not evaporate, leaving the generator to increase. Therefore, although the vapor production with a high concentration of ammonia in the separator tends to increase as the temperature in the generator rises, it cannot compensate for the decrease in the mass flow of refrigerant produced in the generator. For this reason, the total inlet flow to the turbine decreases with an increase in generation temperature.

The cooling effect on the CCPC decreases by having a lower mass flow, as shown in Figure 5, where three evaporation temperatures are analyzed. At a T_E = 5 °C, increasing T_G from 110 to 150 °C causes a decrease in the cooling effect by 34%, from 369 kW to 244.1 kW. Due to the decrease in $\dot{Q}_E$, it is expected that $\dot{W}_T$ would have a similar effect due to the decrease in mass flow due to the increase in T_G. However, in Figure 5, there is an increase in $\dot{W}_T$ as T_G increases. This is because although refrigerant production in the generator decreases, the refrigerant comes out with a higher amount of energy and at a higher pressure. For this reason, the expansion of the turbine mass flow is higher, and there is an increase in power production. That is, the increase in energy of the working fluid compensates for the decrease in mass flow produced in the generator. It can be seen that the power of the turbine increases from 15.33 kW to 41.64 kW when the generation temperature increases from 110 °C to 150 °C.

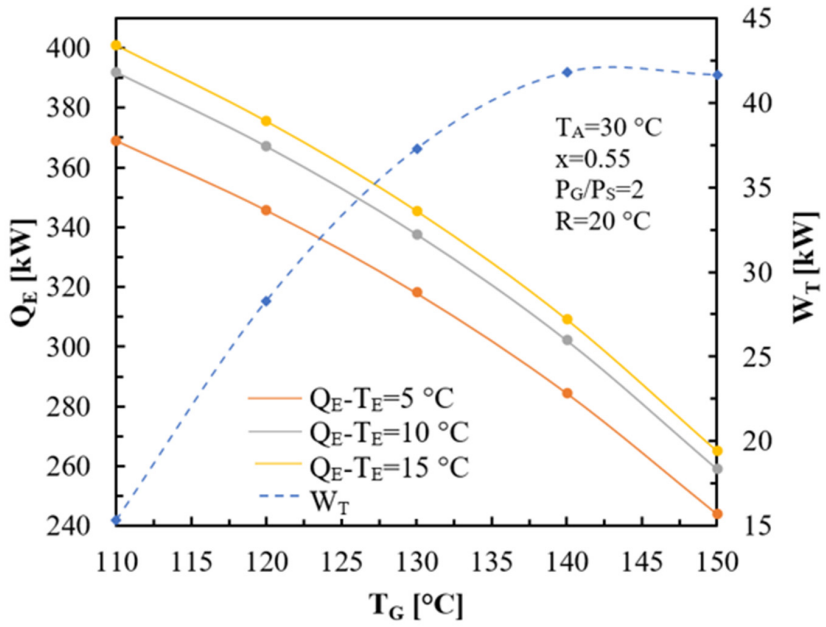

Figure 5. Cooling load and turbine power as a function of the generator temperature.

The *EUF* and exergy efficiencies as a function of the generation temperature are shown in Figures 6 and 7, respectively. Figure 6 shows that the *EUF* is higher at the higher evaporation temperatures but decreases with the increment of T_G. For example, at a T_E = 5 °C, increasing T_G from 110 °C to 150 °C causes the *EUF* to drop by almost 22%, from 0.47 to 0.37. The decrease in *EUF* is mainly the result of the decrease in the mass flow produced in the generator and, therefore, the cooling effect reduction in the CCPC.

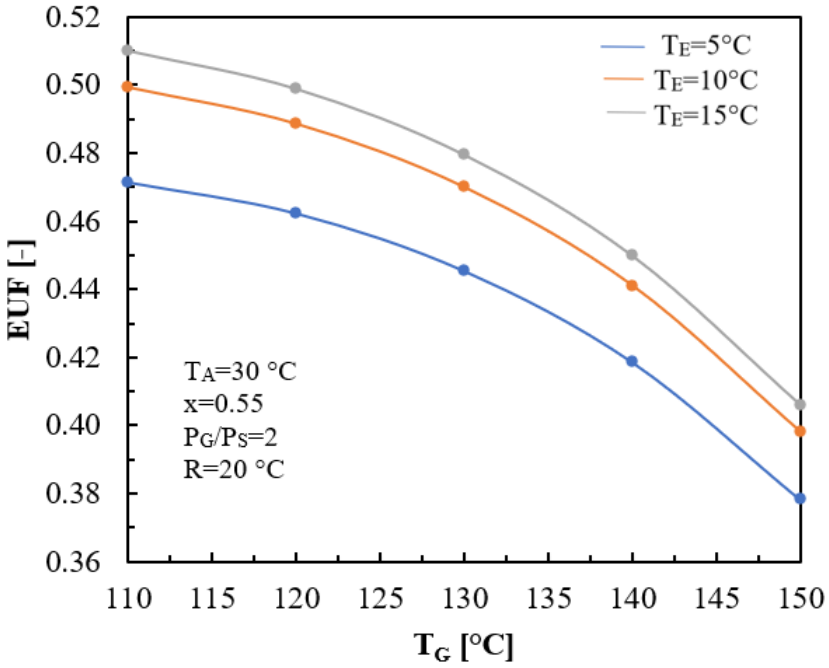

Figure 6. Energy utilization factor as a function of the generator temperature.

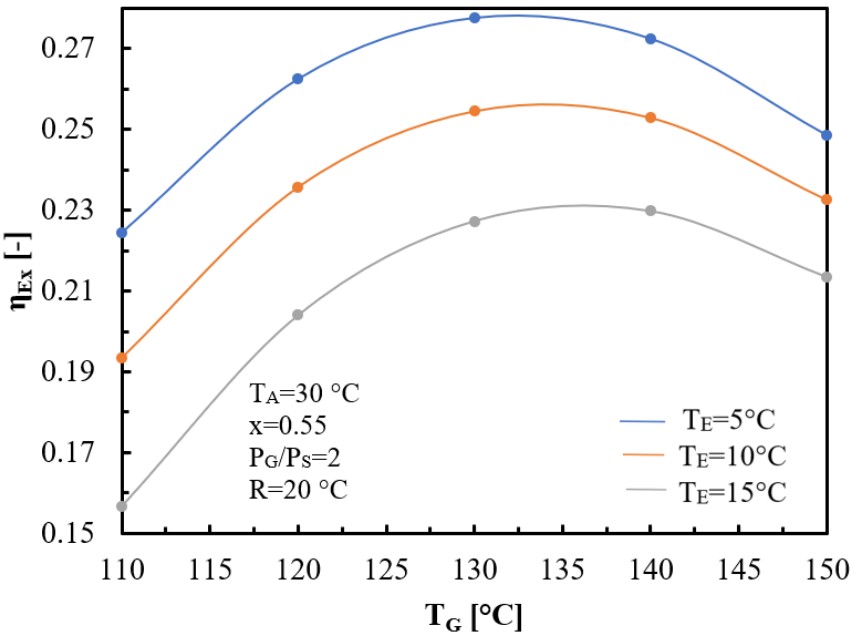

Figure 7. Exergy efficiency as a function of the generation temperature.

In Figure 7, the exergy efficiency of the CCPC increases until it reaches a maximum point and then begins to decrease. The increase in W_T is related to the fact that the fluid at the turbine inlet has a higher pressure and energy; therefore, the expansion process is higher, thus producing more power in the turbine. The fact that the efficiency drops after a maximum point is related to the abrupt decrease of the flow produced in the generator, and although this flow has higher energy, the energy does not compensate for the decrease in mass flow. At T_E = 5 °C, when increasing T_G from 110 °C to 140 °C, the exergy efficiency increases from 0.22 to 0.27, while when increasing from 140 °C to 150 °C, the exergy efficiency decreases from 0.27 to 0.24.

5.2. Analysis of the CCPC as a Function of the Absorption and Condenser Temperatures

From the system assumptions, it was considered that the absorption temperature was the same as the condensation temperature. Figure 8 shows the trend of the cooling load and the power produced by the turbine as the absorber temperature increases. When the absorption and condensation temperature increases, the system pressure also increases since the solution leaving the condenser and the absorber is in saturation conditions. For this reason, if $T_A = T_C$ increases, the expansion process in the turbine decreases, in addition to the fact that the fluid enters the evaporator with a higher amount of energy, thus limiting the evaporation process. For example, when T_A increases from 26 °C to 40 °C at T_E = 15 °C, the cooling load decreases by 16.71%, and $\dot{W}_T$ drops by almost 60%. $\dot{W}_T$ decreased from 384.7 kW to 320.4 kW, while $\dot{Q}_E$ decreased from 33.36 kW to 13.36 kW. On the other hand, it can be seen that at evaporation temperatures below 5 °C, the system cannot carry out the cooling process at absorption temperatures above 30 °C since the working fluid enters the generator at a higher temperature than desired.

With the reduction of the turbine power and the cooling load, the *EUF* and the η_{Ex} decrease. Figures 9 and 10 show the trend of *EUF* and η_{Ex} as a function of T_A, respectively.

Figure 9 shows that the *EUF* presents lower values at relatively high temperatures of $T_A = T_C$ for the absorption and condensation processes. Increasing T_A from 26 °C to 46 °C at a T_E = 10 °C decreased the *EUF* by 8.16%, from 0.497 to 0.455. Also, at a T_E = 10 °C, the system can operate at T_A lower than 36 °C, while at T_E = 5 °C, the maximum absorber temperature is 30 °C.

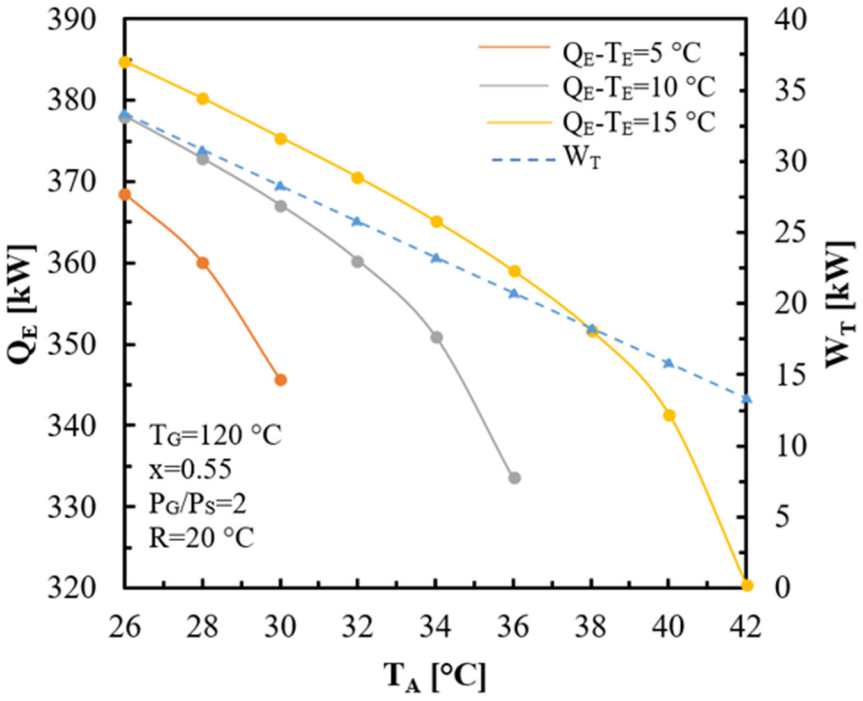

Figure 8. Cooling load and turbine power as a function of the absorber temperature.

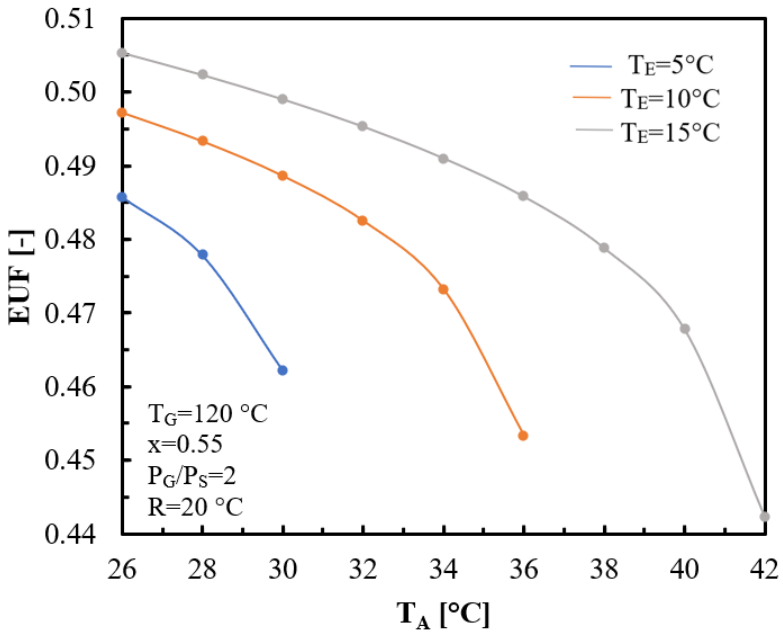

Figure 9. Energy utilization factor as a function of the absorber temperature.

Figure 10 shows that η_{Ex} shows the same tendencies as those shown in Figure 9 for the *EUF*, but η_{Ex} reduces by 24%, decreasing from 0.25 to 0.19.

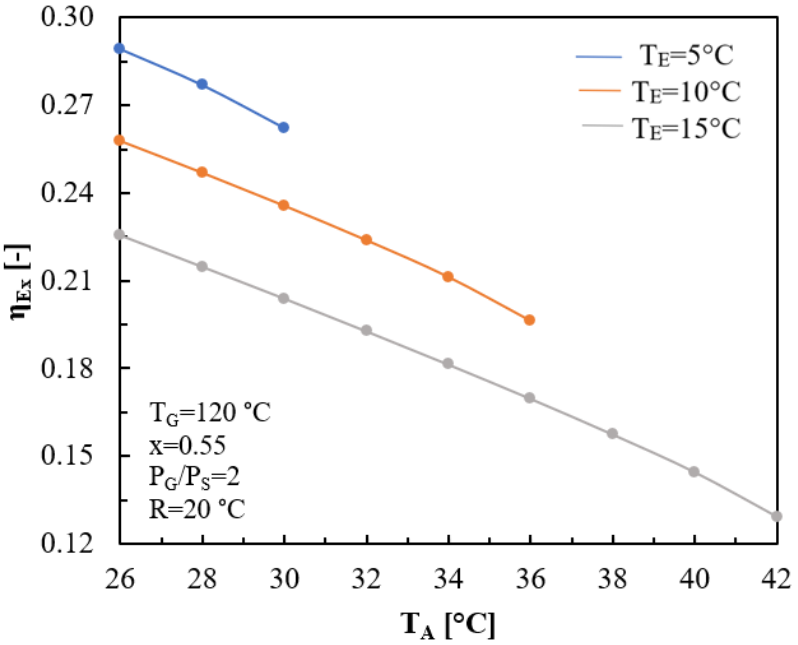

Figure 10. Exergy efficiency as a function of the absorber temperature.

5.3. Analysis of the CCPC as a Function of the Evaporator Temperature

One of the main operating parameters is the system evaporation temperature since the CCPC applications depend on it. Figures 11–13 show the system's analysis as a function of T_E at different reheating temperatures.

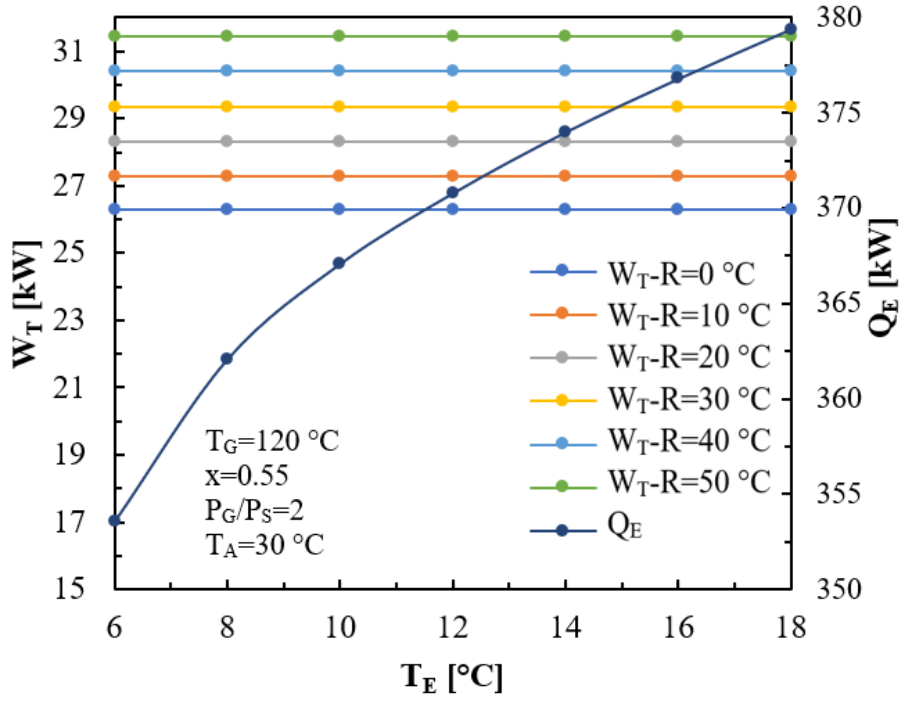

Figure 11. Cooling load and turbine power as a function of the evaporator temperature.

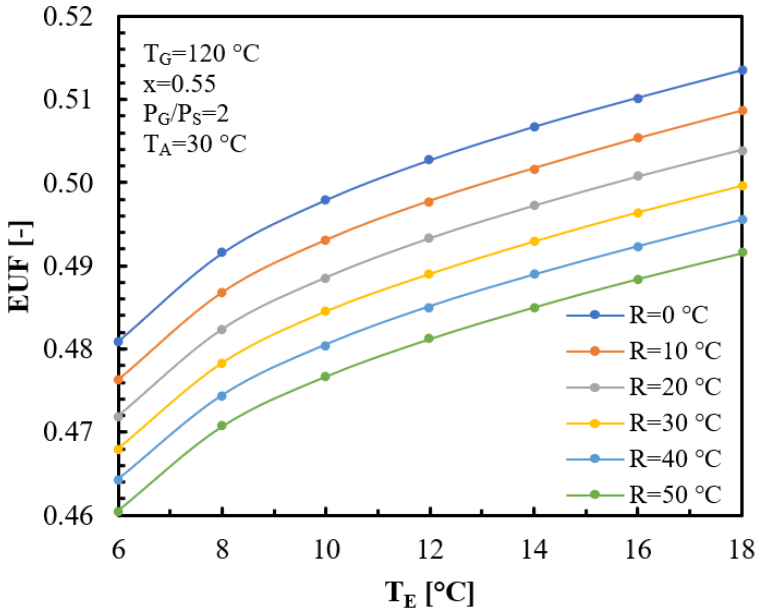

Figure 12. Energy utilization factor as a function of the evaporator temperature.

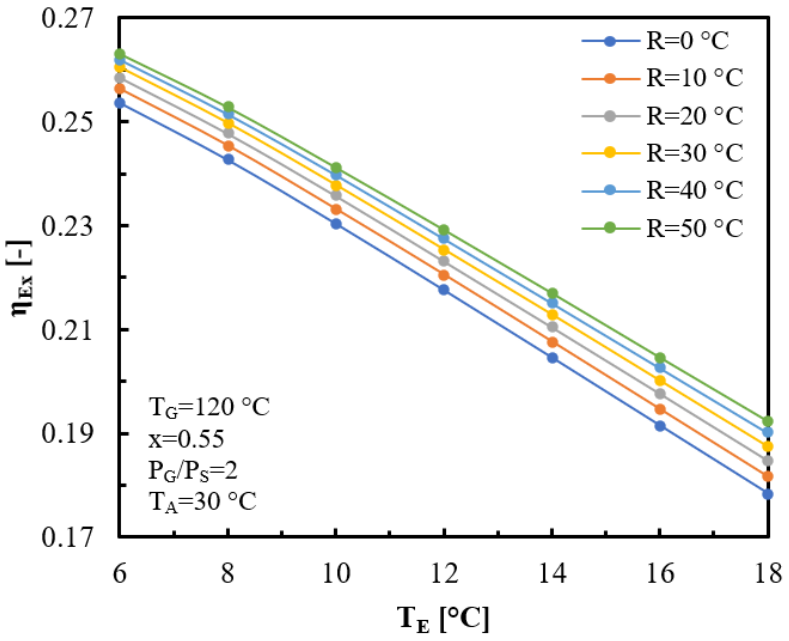

Figure 13. Exergy efficiency as a function of the evaporator temperature.

As shown in Figure 11, the power produced is not affected by the increase in T_E since the conditions of the working fluid at the turbine outlet are delimited by the condenser. On the other hand, the reheating only benefits the power output. When the ammonia in a vapor phase receives a reheat of 50 °C at a T_E = 8 °C, the power production improves by 19.6%, going from a value of 26.28 kW to 31.43 kW. While increasing T_E from 6 °C to 16 °C, the cooling effect improves by 7.3%, from 353.6 kW to 379.4 kW.

In Figure 12, it can be seen that improving the cooling load due to higher reheating temperatures benefits the *EUF*. Figure 12 also shows that higher *EUF* is obtained by increasing the evaporation temperature. At a reheating temperature (*RT*) = 30 °C, increasing T_E from 6 °C to 16 °C increases the *EUF* by 6.52%.

On the other hand, the lowest *EUF* values are found for the cases where the reheating is higher. This is because the energy supplied in the superheater is higher than the benefit

obtained in the turbine. At a T_E = 8 °C and no overheating in the system, the *EUF* is 0.49, but when 50 °C overheats the working fluid, the *EUF* drops to 0.47.

It is expected that the exergy efficiency of the CCPC has the same behavior as the energy utilization factor when increasing the evaporation temperature. However, as seen in Figure 13, the exergy efficiency shows the opposite behavior since the variation of T_E only affects the cooling load produced by the system. At higher evaporation temperatures, the exergy of the cooling load decreases. When the system does not have overheating, the exergy efficiency drops from 0.25 to 0.17 when the T_E increases from 6 °C to 18 °C.

5.4. Comparison of the CCPC with and without Internal Rectification (IR)

Figures 14 and 15 show the comparison of the performance of the CCPC operating with and without internal rectification (IR).

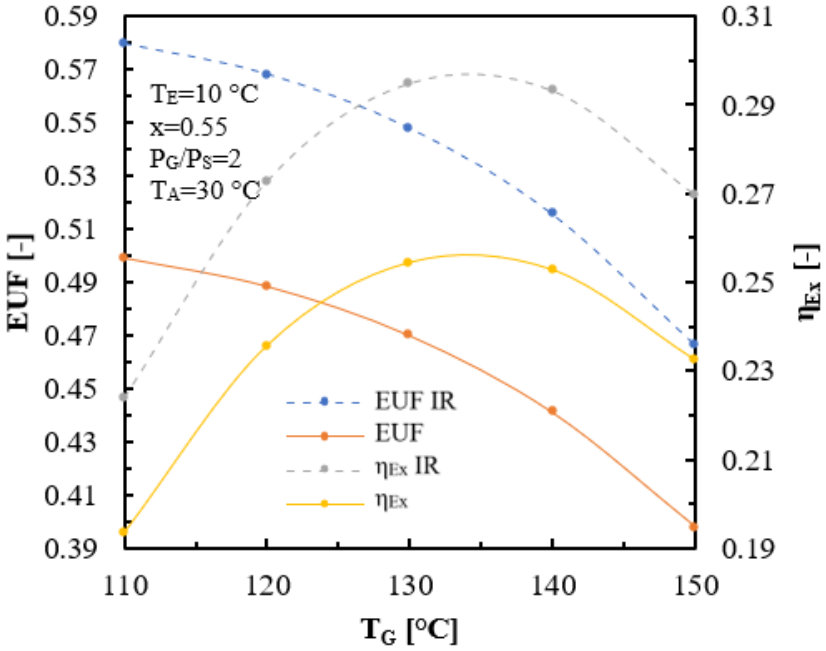

Figure 14. Energy utilization factor and η_{Ex} for the CCPC with and without internal rectification as a function of T_G.

It has been previously discussed that the increment in the generation temperature of the CCPC diminishes the mass flow rate of the vapor phase leaving the generator, and although the increment of T_G benefits the vapor generation in the separator, it does not compensate for the decrement of the desorbed fluid.

In Figure 14, the *EUF* and the η_{Ex} with and without IR are shown as a function of T_G. As mentioned, IR consists of dividing the flow at the pump outlet, where a fraction of the working fluid passes through the rectifier, extracting heat from this component. The IR does not allow the system to increase the power generation or the cooling effect but reduces the heat supplied to the generator. As seen in the figure, this reduction allows the system to achieve higher *EUF* and η_{Ex}. Thus, the *EUF* and the η_{Ex} improve when the system operates with IR. At a T_G = 130 °C, the system without IR reaches an *EUF* of 0.47, while with IR, this parameter reaches 0.54, an increase of almost 15%. Similarly, the η_{Ex} improves from 0.25 to 0.29.

In Figure 15, the *EUF* increases while the η_{Ex} decreases with the increment of T_E because of the reasons previously explained in Figures 12 and 13. Also, it is demonstrated that the system with IR achieves higher *EUF* and η_{Ex} than without IR. At a T_E = 10 °C, the *EUF* is 0.585 with IR, while without IR, it is 0.494, and the η_{Ex} are 0.572 and 0.534, respectively.

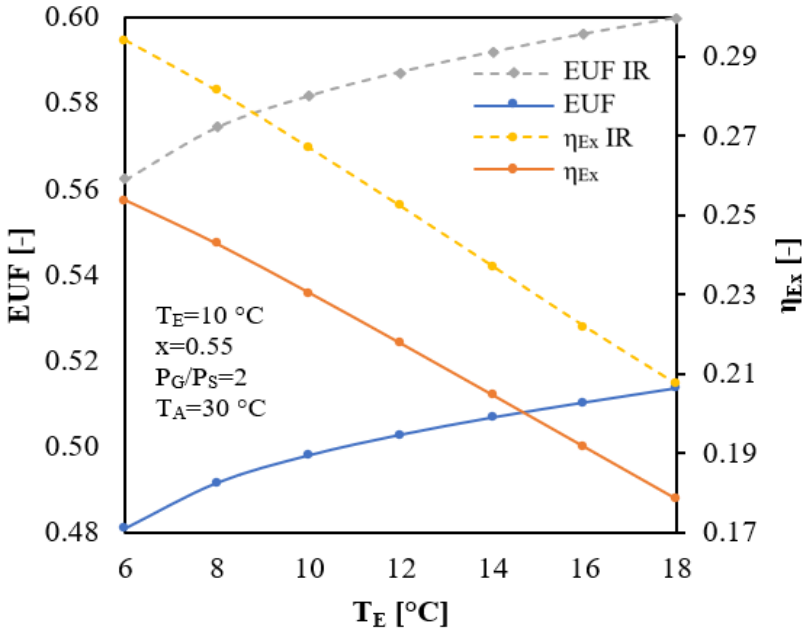

Figure 15. Energy utilization factor and η_{Ex} for the CCPC with and without internal rectification as a function of T_E.

5.5. Analysis of EUF as a Function of X_A

Figure 16 shows the energy utilization factor of the system as a function of X_A for different T_E. When the concentration increases, it can be observed that the *EUF* tends to increase in all the cases analyzed; however, a maximum point is reached, and subsequently, a decay is noted, which is the result of the working fluid entering the evaporator at a temperature almost equal to T_E, causing the cooling effect to not be carried out. When X_A increases from 0.5 to 0.55, with T_E of 0 °C, the *EUF* reaches a value of 0.42 to 0.46. It is important to mention that the temperature of the fluid in the evaporator inlet is almost 2 °C for X_A = 0.55; if the concentration increases, the temperature in this part will decrease, and the cooling effect cannot be produced. It can also be observed that the highest concentration under which the system can operate at evaporation temperatures of 5 °C or higher is 0.55 for the established conditions of T_G and T_A.

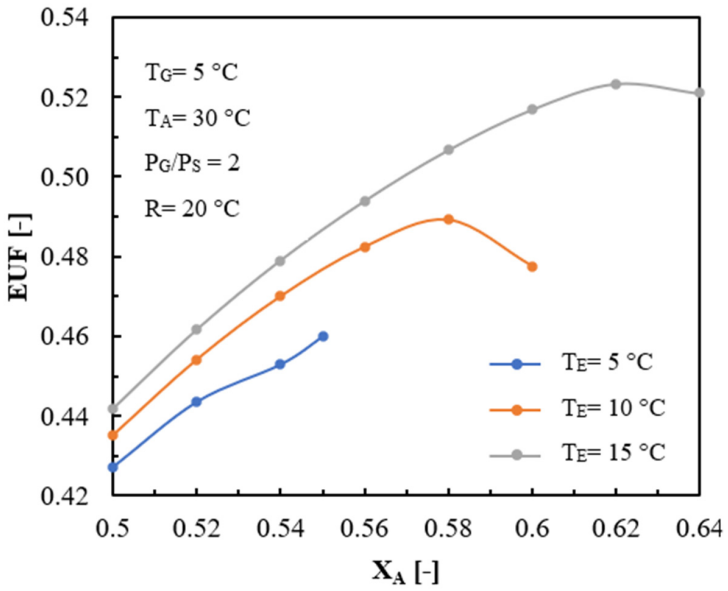

Figure 16. Energy utilization factor as a function of T_{Amb}.

5.6. Analysis of the Ambient Temperature

Figure 17 shows the variation of the exergetic efficiency of the system as a function of ambient temperature (T_{Amb}) for different cases of T_E. As shown in Table 1, η_{Ex} depends on the interactions of power and heat in each component of the system. When T_{Amb} increases, the exergy is related to $\dot{Q}_E$ too; however, the term of exergy for $\dot{Q}_G$ and $\dot{Q}_R$ decreases, and for this reason, η_{Ex} increases when T_{Amb} increases. When the T_{Amb} is 30 °C and the system evaporates at 10 °C, the exergetic efficiency is 0.30, while at the same T_{Amb} but evaporating at 5 °C, the exergetic efficiency is 0.33, which is 10% higher.

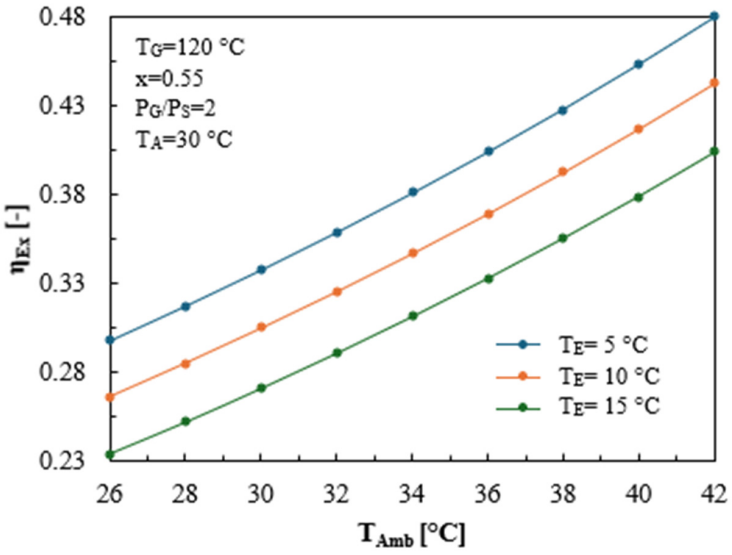

Figure 17. Exergy efficiency as a function of T_{Amb}.

5.7. Analysis of the Irreversibilities of the System with IR

The previous section clearly showed that the CCPC operating with IR is more efficient; therefore, the analyses carried out in this and the following sections are based on this configuration.

An exergy analysis determined that the generator, the evaporator, and the absorber are the components with the highest irreversibility contribution, reaching values up to 38.16 kW, 16.57 kW, and 10.42 kW, respectively. The highest irreversibilities in the generator and evaporator are directly related to the phase change from liquid to vapor. On the other hand, the absorber's highest irreversibility is related to the exothermic reaction product of the ammonia absorption by the solution.

Table 3 shows the irreversibilities for each system component at T_G = 120 °C, T_E = 10 °C, and T_A = 30 °C.

Table 3. Irreversibilities of the system for each one of the components of the CCPC with IR.

Component	I [kW]
Absorber	10.42
Evaporator	16.57
Generator	38.16
Rectifier	14.37
Condenser	3.63
Economizer	3.65
Turbine	2.65
Other components	6.81

5.8. Economic Analysis of the System

Tables 4 and 5 present the results obtained from the economic analysis of the CCPC with IR. The analysis was conducted at the operating conditions of T_G = 120 °C, T_E = 10 °C, and T_A = 30 °C, at which one of the highest *EUFs* was obtained (0.58).

Table 4. Cost contribution by component.

Components	% Cost
Absorber	13.22
Compressor	8.63
Condenser	47.37
Evaporator	9.45
Turbine	15.31
Other components	5.99

Table 5. Results of the economic analysis for the CCPC and CCPCIR.

Parameter	Unit	Value CCPC	Value CCPC IR
Ztotal	[$]	469,753	453,459
CRF	[-]	0.087	0.087
SFF	[-]	0.015	0.015
ACC	[$]	41,039	39,615
SV	[$]	93,951	90,692
ASV	[$]	1443	1393
MC	[$]	4104	3962
ATC	[$]	43,699	42,134
CCCP	[$/kW]	0.071	0.070

Table 4 shows each component's cost contribution. The condenser has the highest cost, followed by the turbine and the absorber.

Table 5 shows the different costs of the system determined with the equations presented in Section 4.

In Table 5, the capital recovery and the sinking found factors are similar to those reported in the literature [23] since it was considered the same interest rate and the lifetime of the equipment. Utilizing the *CEPCI*, which is a cost correction factor, the system total cost (*Ztotal*) is $469,753, which increased by 65% compared with the cost that the system could have had in the year 2000. On the other hand, the salvage value was considered 20%, which means that at the end of the system lifetime, $93,951 could be recovered.

To show the relevance of the proposed system, its performance is compared with the Goswami cycle [30], which is also proposed for the simultaneous production of power and cooling.

Table 6 shows a comparison of the proposed system with the Goswami, both operating with IR at similar operating conditions (T_G = 127 °C, T_A = 7 °C, T_E = 7 °C, and X_A = 0.53). From this table, it can be seen that although the power produced with the proposed cycle is almost half of that of the Goswami cycle, the cooling load is about nine times higher with the proposed cycle, increasing from 25.9 kW to 228 kW, thus achieving a considerably higher *EUF* of 0.61. It is almost three times higher than that with the Goswami cycle. The significant difference in the cooling loads results from the extra mass flow rate produced by the added components to the CCPC. It is important to mention that the exergy efficiency of the Goswami cycle was not reported in the original work; this was calculated using the operating conditions reported in the investigation of Xu et al. [30]. The results shown in Table 6 clearly show that the highest η_{Ex} is obtained with the Goswami cycle since a higher power is produced with this system. However, the cooling effect is too low compared with the proposed system, which can produce almost ten times more cooling than the Goswami cycle, thus increasing the *EUF*.

Table 6. Comparison of the proposed system's performance with the Goswami cycle with IR.

Parameter	Goswami with IR [30]	Present Model
$\dot{Q}_G$ [kW]	390.4	390.1
$\dot{Q}_R$ [kW]	31.3	26.48
$\dot{Q}_E$ [kW]	25.9	228
$\dot{W}_T$ [kW]	76	39.72
$\dot{W}_B$ [kW]	2.7	1.87
EUF	0.23	0.61
η_{Ex}	0.70	0.42

In order to evaluate the results obtained from the proposed system's modeling and economic analysis, the CCPC was compared with a system for the same purposes recently proposed by Shankar and Rivera [23]. The results of this comparison are shown in Table 7. The models were compared using the same operating temperatures and the energy supplied to the generator. The table shows that although the exergy efficiency is lower with the proposed system, the power produced by the turbine was more than double, and the cost per kW produced was 0.58, which is 27% lower than the system proposed by the other authors. It is important to mention that, in the system proposed by Shankar and Rivera [23], the cost of the expansion valves was not considered, and they did not consider the *CEPCI* index.

Table 7. Comparison of the proposed system with the system proposed by Shankar and Rivera [23].

Parameter	Shankar and Rivera [23]	Present Work
T_G [°C]	140	140
T_E [°C]	15	15
T_A [°C]	35	35
$\dot{Q}_G$ [kW]	773.52	772.8
$\dot{Q}_E$ [kW]	354.21	342.4
$\dot{W}_T$ [kW]	20.28	47.2
$\dot{W}_{Com}$	-	18.56
$\dot{W}_B$	7.71	3.97
EUF	0.47	0.48
η_{Ex}	0.43	0.25
CCPC ($/kW)	0.079	0.058

It is worth noting that the analysis was conducted for a system supplying approximately 400 kW in the generator. However, the system's capacity can be easily scaled up to a higher capacity without significant modifications. This is due to the availability of microturbines and heat exchangers capable of generating megawatts of power [35]. This scalability underscores the potential of the proposed system for future applications.

6. Conclusions

The working fluid entering the turbine decreases with an increment in the generation temperature, reducing the cooling load but augmenting the power production. This happens due to the higher pressure at the turbine inlet, producing a higher expansion process.

By increasing the system's generation temperature, the energy utilization factor decreased due to the reduction in the cooling load. However, the exergy efficiency improved because of the higher power produced by the turbine.

Increasing the condenser and absorber temperatures reduces the production of the working fluid, affecting the cooling effect and the system's power.

Reheating the fluid before entering the turbine only improves the system's power production but has no effect on the cooling load since the condenser temperature limits it.

Internal rectification was found relevant since its use significantly reduces the heat supplied to the generator, thus increasing both the energy utilization factor and the exergy efficiency.

At T_G = 120 °C, T_A = 30 °C, and T_E = 10 °C, the energy utilization factor was 0.58 and the exergy efficiency 0.26. At these conditions, it was observed that the generator, the absorber, and the evaporator were the components with the highest exergy destruction, while the condenser and the absorber were the most expensive components, contributing 28.6% and 7.98% to the total cost, respectively.

Comparing the proposed system with the Goswami cycle revealed that although the power production was about half that in the Goswami cycle, the cooling load increased almost ninefold, going from 25.9 kW to 228 kW, thus considerably improving the energy utilization factor from 0.23 to 0.61.

The comparison with the system proposed by Shankar and Rivera found that for similar operating conditions, the cooling load was almost the same for both systems. However, the power produced with the proposed system was considerably higher, while the cost was approximately 27% lower.

Author Contributions: Conceptualization, W.R., A.P.-R. and R.S.; software, A.P.-R.; economic study, R.S., A.P.-R. and J.A.H.-M.; methodology, W.R., J.C.J.-G. and A.P.-R.; investigation, J.C.J.-G., A.P.-R., W.R. and J.A.H.-M.; writing—original draft preparation, J.A.H.-M., J.C.J.-G. and A.P.-R.; writing—review and editing, J.C.J.-G. and W.R.; visualization, A.P.-R. and J.C.J.-G.; supervision, W.R.; project administration, W.R. All authors have read and agreed to the published version of the manuscript.

Funding: This research received no external funding.

Data Availability Statement: The data presented in this study are available on request from the corresponding author due to the data published were generated by using a License software.

Acknowledgments: Alejandro Pacheco-Reyes thanks CONAHCYT for the doctoral scholarship awarded.

Conflicts of Interest: The authors declare no conflicts of interest.

Glossary

Nomenclature

$\dot{Q}$	Heat
$\dot{W}$	Power
$\dot{m}$	Mass flow

Abbreviations

A	Absorber, Area
ACC	Annual capital cost
ASV	Annual salvage value
ATC	Annual total cost
AP	Actual performance
C	Condenser
CCCP	Cost of cogeneration output by considering annual equivalent electric energy
Com	Compressor
CPSC	Cycle with separator for power and cooling
CRF	Capital recovery factor
d	Destruction
E	Evaporator
Ec	Economizer
EUF	Energy utilization factor
Ex	Exergy
G	Generator
MTP	Modeling test performance
PR	Pressure ratio
R	Reheater/Reheating
Rec	Rectifier
S	Separator
SFF	Sinking fund factor
SV	Salvage value
t	Turbine
V	Valve
Z	Component cost

Thermodynamic properties

h	Enthalpy
P	Pressure
s	Entropy
T	Temperature
X	Concentration

Greek letters

ε	Effectiveness
η	Efficiency

Units

°C	Degrees Celsius

i	Interest rate	J	Joule
MC	Maintenance cost	W	Watt
n	Number of years	Wh	Watt-hour
P	Pump	$	Dollar
Pr	Precooler		

References

1. United Nations. Population. Available online: www.un.org/en/global-issues/population (accessed on 14 June 2024).
2. IEA. *World Energy Balances: Overview*; IEA: Paris, France, 2021. Available online: https://www.iea.org/reports/world-energy-balances-overview (accessed on 14 June 2024).
3. United Nations Environment. Cooling Emissions and Policy Synthesis Report. UNEP—UN Environment Programme. Available online: https://www.unep.org/resources/report/cooling-emissions-and-policy-synthesis-report (accessed on 20 July 2020).
4. Yogi Goswami, D. Solar thermal power technology: Present status and ideas for the future. *Energy Sources* **1998**, *20*, 137–145. [CrossRef]
5. Vijayaraghavan, S.; Goswami, D.Y. On evaluating the efficiency of a combined power and cooling cycle. *J. Energy Resour. Technol.* **2003**, *125*, 221–227. [CrossRef]
6. Sadrameli, S.M.; Goswami, D.Y. Optimum operating conditions for a combined power and cooling thermodynamic cycle. *Appl. Energy* **2007**, *84*, 254–265. [CrossRef]
7. Hasan, A.A.; Goswami, D.Y.; Vijayaraghavan, S. First and second law analysis of a new power and refrigeration thermodynamic cycle using a solar heat source. *Sol. Energy* **2002**, *73*, 385–393. [CrossRef]
8. Rivera, W.; Sánchez-Sánchez, K.; Hernández-Magallanes, J.A.; Jiménez-García, J.C.; Pacheco, A. Modeling of Novel Thermodynamic Cycles to Produce Power and Cooling Simultaneously. *Processes* **2020**, *8*, 320. [CrossRef]
9. Demirkaya, G.; Padilla, R.V.; Fontalvo, A.; Lake, M.; Lim, Y.Y. Thermal and exergetic analysis of the Goswami cycle integrated with mid-grade heat sources. *Entropy* **2017**, *19*, 416. [CrossRef]
10. Vijayaraghavan, S.; Goswami, D.Y. Organic working fluids for a combined power and cooling cycle. *J. Energy Resour. Technol.* **2005**, *127*, 125–130. [CrossRef]
11. Wang, J.; Wang, J.; Zhao, P.; Dai, Y. Thermodynamic analysis of a new combined cooling and power system using ammonia–water mixture. *Energy Convers. Manag.* **2016**, *117*, 335–342. [CrossRef]
12. Cao, L.; Wang, J.; Wang, H.; Zhao, P.; Dai, Y. Thermodynamic analysis of a Kalina-based combined cooling and power cycle driven by low-grade heat source. *Appl. Therm. Eng.* **2017**, *111*, 8–19. [CrossRef]
13. Feng, C.; Yu, Z.; Liang, W.; Wang, D. Energetic, exergetic and economic analysis and multi-objective optimization of two novel ammonia-water absorption combined power and cooling cycles driven by low-grade heat sources. *Energy Convers. Manag.* **2021**, *248*, 114781. [CrossRef]
14. Seckin, C. Thermodynamic analysis of a combined power/refrigeration cycle: Combination of Kalina cycle and ejector refrigeration cycle. *Energy Convers. Manag.* **2018**, *157*, 631–643. [CrossRef]
15. Azariyan, H.; Vajdi, M.; Takleh, H.R. Assessment of a high-performance geothermal-based multigeneration system for production of power, cooling, and hydrogen: Thermodynamic and exergoeconomic evaluation. *Energy Convers. Manag.* **2021**, *236*, 113970. [CrossRef]
16. Kumar, G.P.; Saravanan, R.; Coronas, A. Experimental studies on combined cooling and power system driven by low-grade heat sources. *Energy* **2017**, *128*, 801–812. [CrossRef]
17. Zhang, N.; Lior, N. Methodology for thermal design of novel combined refrigeration/power binary fluid systems. *Int. J. Refrig.* **2007**, *30*, 1072–1085. [CrossRef]
18. Suleman, F.; Dincer, I.; Agelin-Chaab, M. Development of an integrated renewable energy system for multigeneration. *Energy* **2014**, *78*, 196–204. [CrossRef]
19. Ayou, D.S.; Bruno, J.C.; Coronas, A. Integration of a mechanical and thermal compressor booster in combined absorption power and refrigeration cycles. *Energy* **2017**, *135*, 327–341. [CrossRef]
20. Cao, Y.; Dhahad, H.A.; Togun, H.; Hussen, H.M.; Anqi, A.E.; Farouk, N.; Parikhani, T. Effect of working fluids in a novel geothermal-based integration of organic-flash and power/cooling generation cycles with hydrogen and freshwater production units. *Int. J. Hydrogen Energy* **2021**, *46*, 28370–28386. [CrossRef]
21. Shankar, R.; Rivera, W. Modeling of a thermodynamic cycle integrating a dual and a triple-pressure cogeneration cycle. *Appl. Therm. Eng.* **2022**, *201*, 117705. [CrossRef]
22. Parikhani, T.; Ghaebi, H.; Rostamzadeh, H. A novel geothermal combined cooling and power cycle based on the absorption power cycle: Energy, exergy and exergoeconomic analysis. *Energy* **2018**, *153*, 265–277. [CrossRef]
23. Shankar, R.; Rivera, W. Analysis of an integrated thermal separation and flashing cooling cogeneration cycle. *Appl. Therm. Eng.* **2021**, *190*, 116773. [CrossRef]
24. Dhahad, H.A.; Hussen, H.M.; Nguyen, P.T.; Ghaebi, H.; Ashraf, M.A. Thermodynamic and thermoeconomic analysis of innovative integration of Kalina and absorption refrigeration cycles for simultaneously cooling and power generation. *Energy Convers. Manag.* **2020**, *203*, 112241. [CrossRef]
25. Kordlar, M.A.; Mahmoudi SM, S. Exergeoconomic analysis and optimization of a novel cogeneration system producing power and refrigeration. *Energy Convers. Manag.* **2017**, *134*, 208–220. [CrossRef]

26. Ghaebi, H.; Parikhani, T.; Rostamzadeh, H.; Farhang, B. Thermodynamic and thermoeconomic analysis and optimization of a novel combined cooling and power (CCP) cycle by integrating of ejector refrigeration and Kalina cycles. *Energy* **2017**, *139*, 262–276. [CrossRef]
27. Ghaebi, H.; Parikhani, T.; Rostamzadeh, H. A novel trigeneration system using geothermal heat source and liquefied natural gas cold energy recovery: Energy, exergy and exergoeconomic analysis. *Renew. Energy* **2018**, *119*, 513–527. [CrossRef]
28. Wang, Y.; Chen, T.; Liang, Y.; Sun, H.; Zhu, Y. A novel cooling and power cycle based on the absorption power cycle and booster-assisted ejector refrigeration cycle driven by a low-grade heat source: Energy, exergy and exergoeconomic analysis. *Energy Convers. Manag.* **2020**, *204*, 112321. [CrossRef]
29. Abam, F.I.; Briggs, T.A.; Diemuodeke, O.E.; Ekwe, E.B.; Ujoatuonu, K.N.; Isaac, J.; Ndukwu, M.C. Thermodynamic and economic analysis of a Kalina system with integrated lithium-bromide-absorption cycle for power and cooling production. *Energy Rep.* **2020**, *6*, 1992–2005. [CrossRef]
30. Xu, F.; Goswami, D.Y.; Bhagwat, S.S. A combined power/cooling cycle. *Energy* **2000**, *25*, 233–246. [CrossRef]
31. Kalan, A.S.; Ghiasirad, H.; Saray, R.K.; Mirmasoumi, S. Thermo-economic evaluation and multi-objective optimization of a waste heat driven combined cooling and power system based on a modified Kalina cycle. *Energy Convers. Manag.* **2021**, *247*, 114723. [CrossRef]
32. Yu, W.; Xu, Y.; Wang, H.; Ge, Z.; Wang, J.; Zhu, D.; Xia, Y. Thermodynamic and thermoeconomic performance analyses and optimization of a novel power and cooling cogeneration system fueled by low-grade waste heat. *Appl. Therm. Eng.* **2020**, *179*, 115667. [CrossRef]
33. Najjar, Y.S.; Alalul, O.F.; Abu-Shamleh, A. Steam turbine bottoming cycle deterioration under different load conditions. *Therm. Sci. Eng. Prog.* **2020**, *20*, 100733. [CrossRef]
34. Interest Rate. Available online: https://www.banxico.org.mx/SieInternet/consultarDirectorioInternetAction.do?accion=consultarCuadroAnalitico&idCuadro=CA51&sectorDescripcion=Precios&locale=es (accessed on 13 February 2020).
35. Pure World Energy. C1000s Capstone Microturbine. Available online: www.pureworldenergy.com/technology/capstone-products/c1000s-capstone-microturbine/ (accessed on 14 June 2024).